Published online 18 February 2013

Nucleic Acids Research, 2013, Vol. 41, No. 7 ***4159–4170***
doi:10.1093/nar/gkt098

Translational repression of thymidylate synthase by targeting its mRNA

Divita Garg[1,2,3,*], Alexander V. Beribisky[2,3], Glauco Ponterini[4], Alessio Ligabue[5], Gaetano Marverti[5], Andrea Martello[4], M. Paola Costi[4], Michael Sattler[2,3,*] and Rebecca C. Wade[1,6,*]

[1]Molecular and Cellular Modeling Group, Heidelberg Institute for Theoretical Studies (HITS), Schloss-Wolfsbrunnenweg 35, 69118 Heidelberg, Germany, [2]Institute of Structural Biology, Helmholtz Zentrum München, Ingolstädter Landstr. 1, 85764 Neuherberg, Germany, [3]Munich Center for Integrated Protein Science, Biomolecular NMR Spectroscopy, Department Chemie, Technische Universität München, Lichtenbergstrasse 4, 85747 Garching, Germany, [4]Department of Life Sciences, University of Modena and Reggio Emilia, via Campi 183, 41126 Modena, Italy, [5]Department of Biomedical Sciences, Metabolic and Neurosciences, University of Modena and Reggio Emilia, via Campi 287, 41126 Modena, Italy and [6]Center for Molecular Biology (ZMBH), Heidelberg University, 69120 Heidelberg, Germany

Received August 6, 2012; Revised December 22, 2012; Accepted January 28, 2013

ABSTRACT

Resistance to drugs targeting human thymidylate synthase (TS) poses a major challenge in the field of anti-cancer therapeutics. Overexpression of the TS protein has been implicated as one of the factors leading to the development of resistance. Therefore, repressing translation by targeting the TS mRNA could help to overcome this problem. In this study, we report that the compound Hoechst 33258 (HT) can reduce cellular TS protein levels without altering TS mRNA levels, suggesting that it modulates TS expression at the translation level. We have combined nuclear magnetic resonance, UV-visible and fluorescence spectroscopy methods with docking and molecular dynamics simulations to study the interaction of HT with a region in the TS mRNA. The interaction predominantly involves intercalation of HT at a CC mismatch in the region near the translational initiation site. Our results support the use of HT-like compounds to guide the design of therapeutic agents targeting TS mRNA.

INTRODUCTION

Thymidylate synthase (TS) catalyzes the reductive methylation of 2′-deoxyuridine-5′-monophosphate (dUMP) to 2′-deoxythymidine-5′-monophosphate (dTMP). It plays a key role in the biosynthetic pathway that, in human cells, provides the sole *de novo* source of thymidylate. As thymidylate is an essential precursor required for DNA replication and repair (1), TS is an attractive anti-cancer target. Drugs inhibiting the TS protein lead to its overexpression and consequent development of drug resistance. The effect has been attributed, at least in part, to the interruption of the autoregulatory feedback loop caused by disruption of the TS protein–TS mRNA interaction (2). Therefore, repression of TS translation by targeting the TS mRNA could provide an effective means of overcoming the development of resistance. The TS-mRNA sequence spanning nucleotides 75–110, referred to as Site I, encompasses the start codon and has been shown to be relevant for the TS mRNA–protein interaction. It is predicted to have a stable stem-loop structure with a CC mismatch in the stem (Figure 1A) (3). Published literature on the interactions of ligands, such as aminoglycosides and HOECHST 33258 (HT) (Figure 1C), with Site I-like RNA constructs (4–6) suggests that these bind at or in the vicinity of the CC mismatch. Therefore, Site I provides a functionally relevant structural motif that may be targeted to develop novel anti-cancer drugs.

HT is a fluorescent dye widely known to bind at the minor groove of AT-rich B-DNA (7). The HT-DNA complex is suggested to be stabilized by hydrogen

*To whom correspondence should be addressed. Tel: +49 6221 533247; Fax: +49 6221 533298; Email: Rebecca.Wade@h-its.org
Correspondence may also be addressed to Divita Garg. Tel: +1 858 784 7758; Fax: +1 858 784 7714; Email: Divita.Garg@tum.de
Correspondence may also be addressed to Michael Sattler. Tel: +49 89 28913418; Fax: +49 89 289 13869; Email: Sattler@helmholtz-muenchen.de
Present addresses:
Divita Garg, The Scripps Research Institute, 10550 North Torrey Pines Road, MEM-131, La Jolla, California 92037, USA.
Alessio Ligabue, Turku Centre for Biotechnology, Åbo Akademi University and University of Turku, Tykistokatu 6, 20520 Turku, Finland.

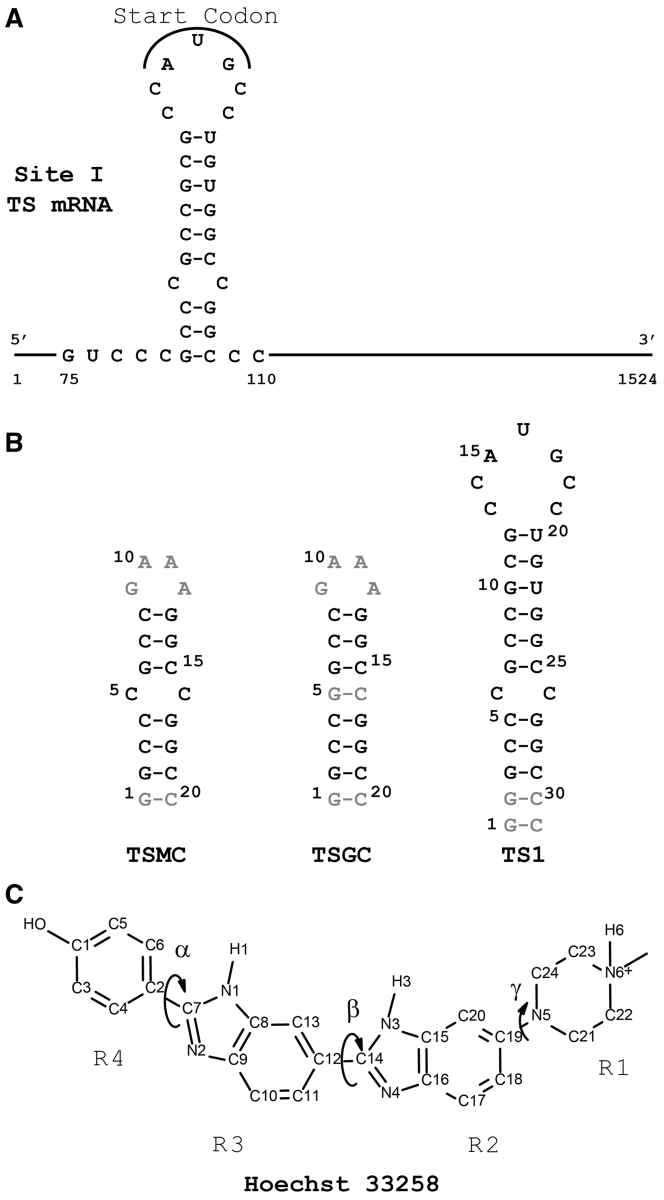

Figure 1. **(A)** Depiction of TSmRNA with the predicted stem-loop secondary structure of Site I (nucleotides 75–110) containing the start codon. **(B)** Predicted secondary structures of the RNA constructs, TSMC, TSGC and TS1. The sequence and structural elements of Site I preserved in the RNA constructs are shown in black, whereas the rest of the RNA construct is gray. **(C)** 2D structure of Hoechst 33258 (HT) with the atom, ring and torsion angle nomenclature used in the text.

bonding and van der Waals interactions with the deep minor groove of B-form DNA helices. However in GC-rich DNA regions, partial intercalation has been observed (8–10). Based on electric linear dichroism studies, HT has also been proposed to intercalate at the pyrimidine bulge in the TAR RNA of HIV-1, although the authors questioned the structural viability of intercalation due to the steric hindrance of the bulky methylpiperazine and hydroxyl phenyl groups on either side of the bis-benzimidazole fragment of HT (11). HT is readily taken into cells and is known to have moderate anti-leukemic and anti-helminthic activity, although the mechanism of cytotoxicity is not well understood (12). HT has been observed to bind specifically to a TS RNA Site I construct with a dissociation constant of 60 ± 13 nM; the binding is facilitated by the presence of a CC mismatch and competitive with binding of the aminoglycoside, paromomycin (4). Mutation and RNase footprinting experiments indicated that the specific binding of HT required non-duplex RNA, was favored by the presence of GC base pairs adjacent to the mismatch but not sensitive to the base type at the bubble (4).

To investigate the biological relevance of the interaction of HT with the TS mRNA, we performed cell-based assays and monitored the effect of HT on the levels of TS mRNA and protein. Surprisingly, we observed that HT reduced the TS protein levels by acting at the level of translational regulation, raising the possibility that HT might directly interact with the TS mRNA in the cell. To exploit HT as a lead compound for the design of anti-cancer agents targeting the TS mRNA, a detailed structural characterization of HT-mRNA binding is desirable. Since the CC-mediated HT binding site on TS mRNA (4) is distinct from the HT binding site observed for the TAR RNA (11), a direct deduction of the binding mode from that for TAR RNA is not feasible. We therefore studied the molecular details of HT-TS mRNA interactions using nuclear magnetic resonance (NMR), UV-Vis and fluorescence spectroscopy techniques, complemented with computational docking and molecular simulations. For this purpose, we analyzed three RNA constructs: TS1, TSMC and TSGC (Figure 1B). TS1 has the native predicted stem loop structure of Site I, stabilized by two additional GC base pairs; its interaction with HT was reported by Cho *et al.* (4). TSMC is a shorter construct that has the same three base pairs as Site I flanking the CC mismatch in both directions; its interaction with paromomycin has previously been studied by NMR (6). The CC mismatch of TSMC has been replaced by a GC base pair in TSGC. Our data show that HT binds the Site I-like RNA constructs in an ensemble of modes with intercalation at the site of the CC bubble being the dominant binding mode.

MATERIALS AND METHODS

Materials

RNA oligonucleotides

TSMC 5′-(r(GGC CCG CCG AAA GGC CGG CC))-3′, TSGC 5′-(r(GGC CGG CCG AAA GGC CGG CC))-3′ and TS1 5′-(r(GGG CCC GCC GCG CCA UGC CUG UGG CCG GCC C))-3′ were purchased from Biospring GmbH, Frankfurt, Germany. The RNA was extensively dialyzed in 500 Da dialysis membrane tubes against progressively decreasing NaCl concentrations (1–0 M) and subsequently lyophilized. Just before measurements, the samples were dissolved and subjected to heating at 95°C for 5 min followed by snap cooling on ice with the aim of trapping the kinetically favored intramolecular monomeric hairpin conformation rather than an intermolecular dimer. The stoichiometry of the samples was checked with native PAGE.

DNA oligonucleotides

AT-DNA (5′-AAG GCT ACG ATC CGC ATC CGA AAA TTA AAG CGC CGG TGG CTA T-3′/5′-TTC CGA TGC TAG GCG TAG GCT TTT AAT TTC GCG GCC ACC GAT A-3′) and GC-DNA (5′-GCG GCC GC-3′) were purchased from Eurofins MWG Operon, Ebersberg, Germany. Just before measurements, the samples were dissolved and subjected to heating at 95°C for 5 min followed by slow cooling to room temperature to favor the formation of a duplex.

HT

HT was purchased from Sigma Aldrich (ID B1155).

Cell line

The 2008 cell line was established from a patient with serous cystadenocarcinoma of the ovary. The cells were grown as monolayers in RPMI 1640 medium containing 10% heat-inactivated fetal bovine serum and 50 μg/ml gentamycin sulfate. All cell media and serum were purchased from Lonza, Verviers, Belgium. Cultures were equilibrated with humidified 5% CO_2 in air at 37°C. All studies were performed in Mycoplasma negative cells, as routinely determined with the MycoAlert Mycoplasma detection kit (Lonza, Walkersville, MD, USA).

Methods

Biological assays

Drug treatment. The cells were administered with increasing concentrations of HT (0, 0.1, 1, 2.5, 5, 7.5, 10 and 20 μM) and incubated for 48 and 72 h. In addition, the compound N1,N12,bis(ethyl)spermine (BESpm) was administered to the cells and incubated for a period of 72 h as a control. BESpm is a bis(ethyl) analog of the naturally occurring polyamine spermine. It has been shown to downregulate the key enzymes for polyamine biosynthesis, ornithine decarboxylase and S-adenosylmethionine decarboxylase, and to induce the activity of the rate-limiting enzyme in polyamine catabolism, spermidine/spermine N^1-acetyltransferase, resulting in depletion of polyamine pools and inhibition of cell growth at micromolar concentrations in several tumor models (13). Since, no effect of BESpm alone on TS expression has been reported, the compound was chosen as a control molecule to confirm the specific activity of HT.

Western blotting. Cells were harvested, washed twice in ice-cold 1× PBS, resuspended in 20 mM Tris-HCl (pH 7.4), 150 mM NaCl, 1 mM EDTA (pH 8.0), 1% Triton X-100 and 0.1% SDS and lyzed by freeze–thawing three times followed by sonication using three 2−3 s bursts. The insoluble debris was removed by centrifugation at 15 000 × g for 30 min. Protein concentrations were determined using the method of Lowry (14). In total, 25 μg of each protein sample was resolved by SDS–PAGE (12%). The gels were electroblotted onto hydrophobic polyvinylidene difluoride membranes (HybondTM-P PVDF, GE Healthcare Bio-Science, Uppsala, Sweden). Antibody staining was performed with a chemiluminescence detection system (ECL Plus Western Blotting Detection Reagent, GE Healthcare Bio-Science), using a 1:500 dilution of the anti-human TS mouse TS106 monoclonal primary antibody (Invitrogen S.r.L., Milan, Italy), 1:10 000 of anti-human vinculin mouse antibody for normalization (Sigma-Aldrich S.r.L., Milan, Italy) and 1:3000 dilution of a horseradish peroxidase-conjugated sheep anti-mouse secondary antibody (GE Healthcare Bio-Science). Quantitation of signal intensity was performed by densitometry on a GS-800 calibrated densitometer (Bio-Rad, CA, USA) and analyzed using Quantity One software (Bio-Rad). The protein expression of the housekeeping gene vinculin was used as a control to normalize the measured protein levels.

Real-time reverse transcription-PCR analysis. Total RNA was extracted from the cultured cells using TRI reagent (Sigma-Aldrich S.r.L.). Reverse transcription was performed with 2 μg of total RNA using random primers (Promega, Milan, Italy) and M-MLV reverse transcriptase (Promega). Real time RT-PCR was performed with 10 ng of cDNA using Power SYBR® Green PCR Master Mix [Applied Biosystems, Monza (MI), Italy] and an ABI PRISM 7900 HT Sequence Detection System (Applied Biosystems), followed by a dissociation curve analysis and subsequent agarose gel electrophoresis to confirm amplification. The following TS primers (Genbank: NM_001071.1) were used, forward: 5′-CAG ATT ATT CAG GAC AGG GAG TT-3′ and reverse: 5′-CAT CAG AGG AAG ATC TCT TGG ATT-3′. The amount of target, normalized to an endogenous reference [glyceraldehyde-3-phosphate dehydrogenase (GAPDH)] and relative to a calibrator (untreated sample), was given by $2^{-\Delta\Delta Ct}$ calculation (15). All experiments were carried out three times in triplicate; amplification plots were analyzed using the ABI Prism 7900 HT SDS version 2.1 software (Applied Biosystems).

NMR spectroscopy

RNA samples were measured at 100 μM concentration, in 90% H_2O + 10% ^2H_2O or 100% ^2H_2O, as required and adjusted to pH 6.4 with dilute HCl/NaOH. HT was dissolved at 10 mM concentration in the same solvent as the RNA, and the pH was adjusted to 6.4.

RNA chemical shift changes upon HT addition were monitored using homonuclear 2D Total Correlation Spectroscopy (TOCSY) (16,17) (τ_m = 80 ms) and 2D Nuclear Overhauser Effect Spectroscopy (NOESY) (18) (τ_m = 300 and 80 ms) experiments at HT/TSMC ratios of 0:1, 0.5:1, 1:1 and 1.5:1. Significant precipitation at the highest ratio precluded the use of further titration points. All experiments were performed on a 900-MHz Bruker spectrometer with a cryogenically cooled probe. Measurements were done at 293 K which was found to be the optimal temperature for both water and ^2H_2O measurements. The chemical shift assignments for the free TSMC reported by Tavares *et al*. (6) were used.

UV-Vis, fluorescence spectroscopy

All samples were prepared in 20 mM phosphate buffer solution at pH 7.5. Absorption spectra were measured with a Varian Cary100 dual beam spectrophotometer. Fluorescence spectra were measured with a FluoroMax2

Spex Jobin-Yvon spectrofluorometer. Emission spectra were corrected for the spectral sensitivity of the emission channel; excitation spectra were normalized relative to the spectral intensity distribution of the xenon lamp; the correctness of the procedure was checked in the 300–390 nm region by comparing the absorption and excitation spectra of anthracene in *n*-hexane. All measurements were performed in $0.4 \times 1\,cm^2$ cuvettes at 19–21°C.

Time-correlated single photon counting experiments were performed with an IBH System 5000 equipment having a time resolution around 0.25 ns after deconvolution. The fluorescence decay functions were deconvoluted from the measured time profiles using a combined linear and non-linear iterative reconvolution method based on minimization of the chi-square parameter.

Computational modeling

Preparation and parameterization of the starting structures. Model 6 from the solution structure ensemble of TSMC reported by Tavares *et al*. (PDB ID 2RPT) (6) and HT coordinates from solvation dynamics studies kindly supplied by Dr S.A. Corcelli (19) were used for modeling the complex of TSMC with HT. HT was manually docked (visualization was done in Pymol 1.2r2) in the major groove at the crevice formed by the CC mismatch. Since the orientation of HT with respect to RNA was not known, two docking poses rotated 180° with respect to each other were generated (Supplementary Figure S1). The Parmbsc0 force field (20) was used to parameterize the RNA, and the published parameters (19) were used for HT.

Molecular dynamics simulations. All molecular dynamics (MDs) simulations were performed under periodic boundary conditions using the SANDER module of AMBER10 (21). Water molecules were modeled with the TIP3P (22) potential, and the system was neutralized with Na^+ ions. Electrostatic interactions were computed using the particle mesh Ewald method for which the direct sum cutoff was set to 9 Å. Non-bonded interactions were also cutoff at 9 Å. Bonds involving hydrogen atoms were constrained to their equilibrium lengths using the SHAKE (23) algorithm. Newton's equations of motion were integrated every 2 fs. A variant of a previously reported protocol (24) was used to minimize, heat and equilibrate the systems (Supplementary Figure S2). All simulations were performed in the NPT ensemble. A constant temperature of 300 K was maintained by weak coupling to an external bath (25) with a time constant of 5 ps. The pressure was maintained at 1 atm by isotropic position scaling.

A two-step procedure was used to simulate the complex. In the first step (referred to as A1 and B1, for the docking poses in Supplementary Figure S1A and B, respectively), the fully flexible HT was allowed to explore the surface of a restrained TSMC structure and find an optimal docking pose. This was accomplished by harmonically restraining the atoms of TSMC with a force constant of 25 kcal/mol/$Å^2$, while allowing HT and the solvent atoms to move freely during a production run of 10 ns. The final frame from the A1 step was taken as the initial frame for the second step (referred to as A2) in which induced fit of the HT-TSMC interaction at the CC mismatch was explored. This was accomplished by allowing unrestrained movement of HT, solvent and residues 4–6 and 16–18 of TSMC, i.e. of the CC mismatch and one flanking base pair above and below the mismatch, while the rest of the RNA was harmonically restrained with a force constant of 10 kcal/mol/$Å^2$, during a production run of 24.6 ns. The conformations sampled during the first 5 ns and the last 500 ps of the A2 run were independently averaged and then minimized using steepest descent and conjugate gradient methods to obtain representative models for HT-TSMC groove binding (Figure 2A) and HT-TSMC intercalation (Figure 2B) complexes, respectively.

To estimate the binding free energy for the RNA-ligand interaction, continuum solvent calculations were performed using the internal Poisson-Boltzmann Surface Area (PBSA) solver in Sander in the Amber9 package. To compute binding free energies for the groove bound mode, the intercalation mode and the intermediate transition phase, the trajectory from the A2 run was split into segments of 5 ns each (the last segment being 4.6 ns) which were then used independently for the calculations. The structures of unbound TSMC and HT were taken from the simulated complexes, i.e. changes in the conformation of each of the components were neglected for the binding free energy calculations.

For reference, the unbound forms of TSMC and of HT were simulated for 9 and 2 ns, respectively, using the same settings as for the A2 run.

RESULTS AND DISCUSSION

HT-induced translational repression of TS mRNA

Cell-based assays were conducted to monitor the TS protein and mRNA levels at different administered doses of HT in an ovarian cancer cell line. The TS mRNA levels were essentially unaltered after HT exposure, whereas the TS protein levels were progressively reduced to 25 and 17% of the control on administration of increasing doses of HT for 48 and 72 h, respectively (Figure 3), suggesting that HT affects intracellular TS protein levels by translational regulation. This observation is unanticipated considering that HT is a strong DNA binding compound and therefore expected to preferentially modulate transcription. In addition, since the expression of the vinculin protein remained unaltered, and the control compound BESpm did not reduce TS expression as much as HT (Supplementary Figure S3), the observed effect of HT on TS shows specificity. It has already been shown that HT can bind at the stem of Site I-like RNAs (4,6) and we thus hypothesize that direct interaction with TS mRNA could be a possible mechanism for the HT-mediated repression of TS translation. To obtain detailed structural insights into the HT-Site I interaction, we next pursued experiments using the TSMC construct as a model for the stem of the Site I RNA (Figure 1A and B).

CC mismatch in RNA is the binding site for HT

The prediction of a stem-loop structure for Site I, with a CC mismatch in the stem and the start codon in the loop,

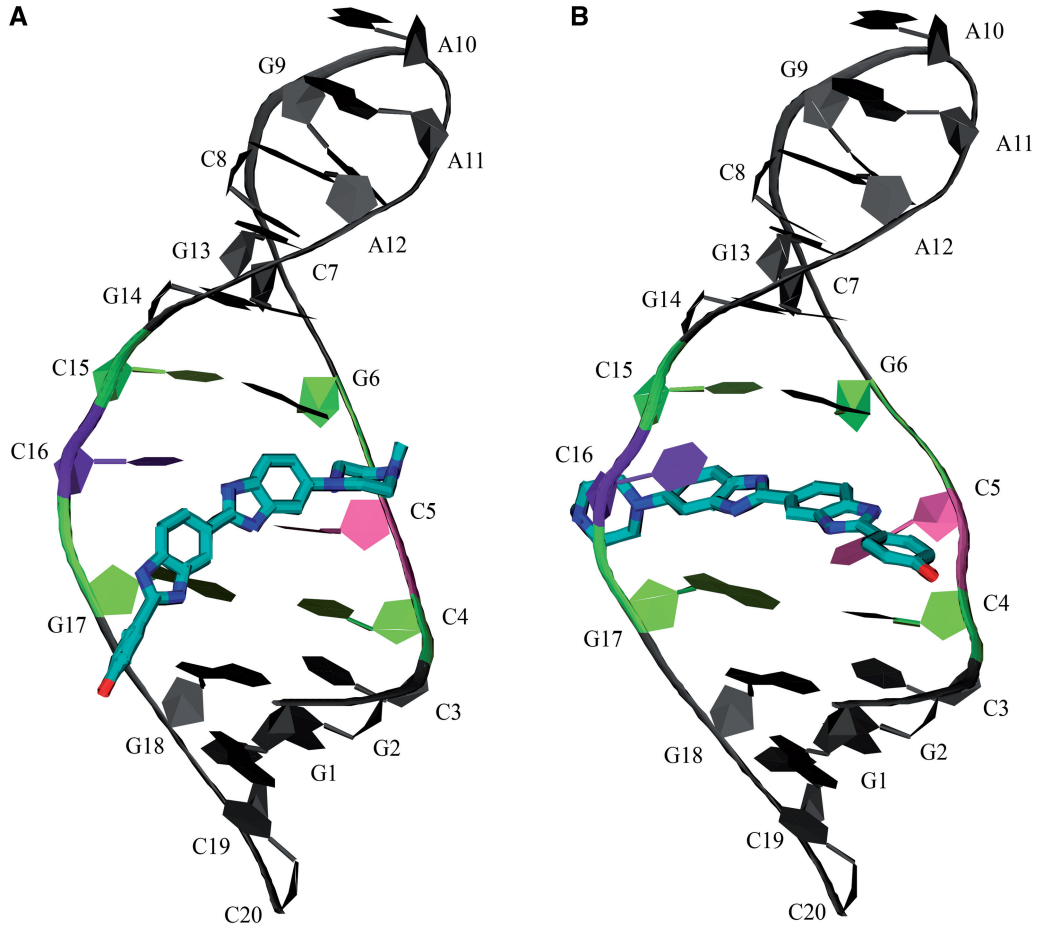

Figure 2. Structural models of **(A)** the groove binding HT-TSMC complex generated by averaging and minimizing the first 5 ns of the simulation A2. TSMC is depicted as a cartoon with the major groove facing the reader, whereas HT is shown in stick representation (C: cyan, N: blue, O: red); and **(B)** the HT-TSMC intercalation complex generated by averaging and minimizing the last 500 ps of the simulation A2.

was first reported by Chu *et al.* (3). In agreement with the prediction, a Site I-like RNA construct was reported to have a high melting temperature of 65°C independent of the concentration, suggesting an intra-molecular stem-loop fold (26). Another Site I-like RNA construct was also observed to adopt a stem-loop fold by solution fluorescence studies, although an asymmetric dimer of two hybridized RNA strands was obtained in the crystal (27). These reports suggest that the Site I indeed adopts a stem-loop structure in solution. Tavares *et al.* (6) have recently reported the NMR structure of a shorter construct, TSMC, and mapped the binding site for the aminoglycoside, paromomycin. In TSMC, the three flanking base pairs on either side of the CC mismatch in the Site I stem are preserved and the resulting stem sequence is capped with a stable GNRA (G = guanine, N = any nucleotide, R = purine, A = adenine) tetraloop (Figure 1B).

TSMC was used to study the structural features of the RNA-HT complex by NMR. A ^{1}H TOCSY experiment, recorded in $^{2}H_2O$, was used to monitor H6/H5 cross-peaks for the pyrimidine residues (exclusively cytosines in the case of TSMC). An overlay of TOCSY spectra recorded in the presence of increasing concentrations of HT is shown in Figure 4. The H6/H5 correlations for C19 and C20 experienced negligible changes in chemical shifts compared with the remaining cytosine residues, suggesting that the binding event occurred at a position distant from the base of the stem. Signal broadening was observed for the H6/H5 correlations of C15, and to a lesser extent, for the joint signal of C16 and C7. Presumably, these residues experience exchange-broadening motions when TSMC is bound to HT. These chemical shift perturbations (CSPs) suggest that the major interaction site between HT and TSMC is the RNA's CC mismatch.

To further investigate the role of the CC mismatch in HT binding, an additional RNA construct, termed TSGC (Figure 1B) was also used. In this construct, C5 was replaced with G5, thereby eliminating the mismatch and replacing it with a GC base pair. However, assigning this construct proved to be very challenging due to the very high degree of overlap in the NOESY (Supplementary Figure S4D). A few resonances in this experiment, as well in a TOCSY experiment, were assigned tentatively based on the comparison of the characteristic chemical shifts with the TSMC spectra (Supplementary Figure S4). For both TSMC and TSGC, chemical shift changes upon HT addition were observed for adenine resonances

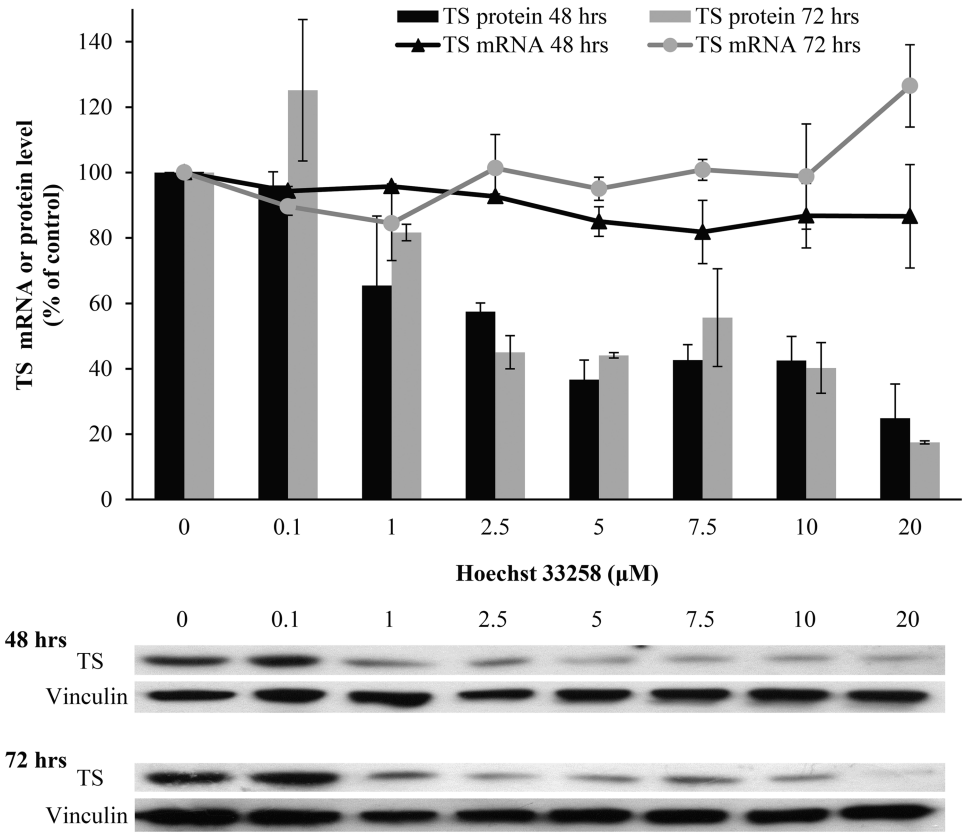

Figure 3. Upper panel: Measured intracellular TS mRNA and TS protein content at increasing HT doses in the 2008 human ovarian cancer cell line. The measurements were done after 48 and 72 h of incubation with HT. The amount of TS mRNA and protein were determined using GAPDH mRNA and vinculin protein as internal references, respectively (see 'Materials and Methods' section). Lower panel: Western blots for TS protein monomer quantification on administration of increasing doses of HT at both time points. Results of a typical experiment, which was carried out twice, are shown.

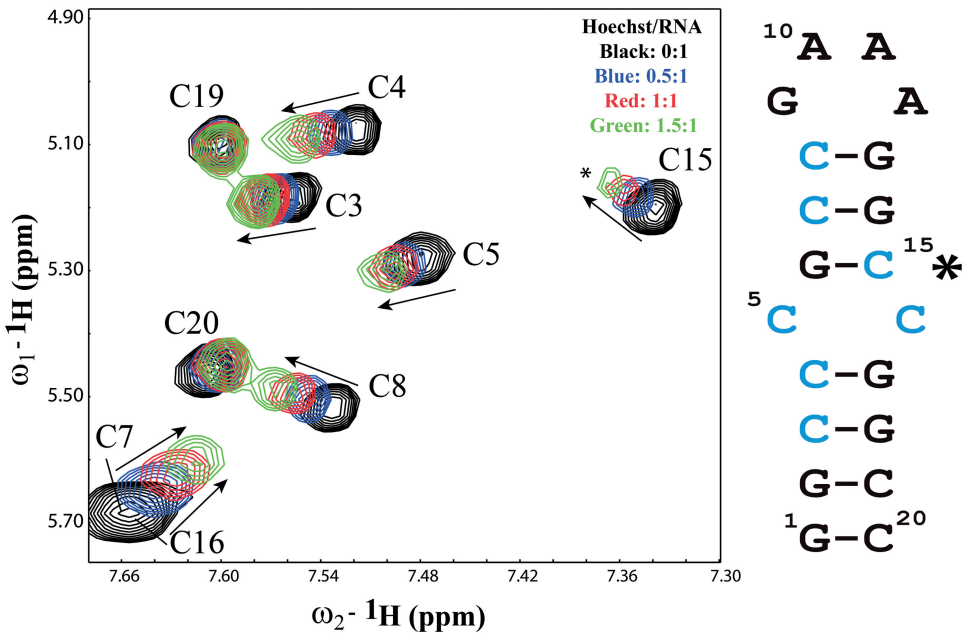

Figure 4. Superposition of 2D ^{1}H TOCSY spectra of TSMC upon addition of HT recorded in $^{2}H_2O$. HT/RNA ratios of 0:1, 0.5:1, 1:1, 1.5:1 are marked in black, blue, red and green, respectively. CSPs induced by HT binding are shown by arrows, the corresponding residues are colored in cyan in the RNA sequence. C15, which experiences a strong CSP and line-broadening, is indicated with an asterisk.

in 2D NOESY spectra (Supplementary Figure S4C and D). In addition, the H6/H5 signals of residue C8 in the TOCSY for TSMC (Figure 4) and (based on tentative assignments) in TSGC (Supplementary Figure S4B) experience significant chemical shift changes. These changes show that HT also interacts with the GNRA tetraloop in both TSMC and TSGC. In addition, the TSMC-HT interaction was studied using a NOESY experiment recorded in H_2O (Supplementary Figure S5). Since every canonical Watson–Crick base pair (except the one at the bottom of the stem) gives rise to a set of cross-peaks in the imino-imino and in the imino-amino regions, chemical shift changes for these protons can be used to determine whether HT binding affects TSMC base pairing. Chemical shift changes for the TSMC RNA were monitored at HT/RNA ratios of 0:1, 0.5:1, 1:1, 1.5:1 and revealed most significant changes for the G17-C4 base pair. G18-C3 G6-C15 and G14-C7 also seem to be affected; however, a high degree of overlap precludes further evaluation. These changes are consistent with our hypothesis that HT binds TSMC at two sites: the CC mismatch and the GNRA tetraloop. The imino-amino signals from all base pairs are conserved at HT/RNA ratios, indicating that the HT addition does not affect TSMC base pair integrity.

Intercalation is the major binding mode of HT to RNA

We were not able to determine a high-resolution NMR structure of the HT-TSMC complex because of a lack of intermolecular Nuclear Overhauser Effects (NOEs), presumably due to the presence of conformational dynamics and multiple interactions of HT with the RNA. The same limitation was reported by Tavares *et al.* for the TSMC–paromomycin complex (6). We therefore used UV-Vis and fluorescence methods to further characterize the interaction of HT with the TS mRNA. HT is fluorescent and thus UV-Vis and fluorescence spectroscopy can report on changes in the environment of HT upon RNA binding, which in turn provides clues about the binding mode. Two binding modes have been characterized in the literature for the interaction of HT with DNA—groove binding at AT-DNA and partial intercalation at GC-DNA (8–10). Therefore, we first characterized the interaction of HT with an AT-rich DNA sample and a GC-rich DNA sample to obtain reference spectroscopic and photophysical datasets for the two binding modes (Supplementary Figures S6 and S7, respectively). Indeed, titration of HT with AT- and GC-DNAs caused different evolutions of the UV-VIS absorption and steady-state and time-resolved fluorescence observables. The main properties of the HT-DNA complexes obtained at large DNA/HT ratios are reported in Table 1. They are consistent with the two mentioned binding modes, as discussed in detail in the Supplementary data.

Binding mode to RNA

In addition to TSMC and TSGC, the RNA construct TS1 (4) was used for these experiments. TS1, has the native Site I sequence and structure stabilized by two additional GC base pairs at the base of the stem and was used as a closer representative of the TS mRNA. Titration of HT with the three RNAs (TSMC, TSGC and TS1) yielded complexes whose spectroscopic and photophysical properties were similar to each other and to those observed upon HT complexation with GC-DNA (Table 1; Figure 5; Supplementary Figures S7–S9). Addition of the RNAs caused a marked emission enhancement (Figure 5A; Supplementary Figures S8 and S9). Like with both HT-DNA complexes, the observation of single-exponential decays and of the independence from the emission and excitation spectra on the excitation and emission wavelengths, respectively, indicated that single emitting HT-RNA complexes were formed. As observed with GC-DNA and, to a smaller extent, HT alone, the excitation spectra of the emitting species were quite strongly red-shifted (from +17 to +21 nm) relative to the absorption spectra obtained at the highest RNA/HT mole ratios achieved (Table 1; Figure 5B); however, titration ends were not reached (Figure 5A; Supplementary Figures S8 and S9). This implies that large amounts of non-fluorescent, likely aggregated species were still present at these RNA/HT ratios, and that these species did not transfer excitation energy to the emitting complexes, i.e. the aggregated and the emitting forms of HT did not coexist within the same HT-RNA molecular complex.

Table 1. Spectroscopic (absorption, emission and excitation maximum wavelengths, λ^m; relative maximum extinction coefficients, ε^m) and photophysical features (relative emission band areas, A^f; and lifetimes, τ) of HT and HT/NA complexes at large NA/HT mole ratios

Nucleic acid	λ^m_{abs} (nm)	ε^m_{HT} $\varepsilon^m_{HT/NA}$	$\lambda_{em}{}^m$ (nm)	$A^f_{HT/NA}$ A^f_{HT}	$\lambda_{exc}{}^m$ (nm)	τ(ns)
None	340	1	510	1	349	0.3 (±0.15)
AT-DNA	352	~1	445	~60	354	2.8
GC-DNA[a]	342	0.8	473	3.8	361	4.1
TSMC-RNA[b]	346	1.2	483	7.7	367	4.2
TSGC-RNA[c]	342	~1.8	480	7.6	360	4.3
TS1-RNA[d]	355	1.4	485	11.1	372	4.1

[a]Values at GC-DNA/HT = 30, evolution not complete.
[b]Values at TSMC-RNA/H = 30, evolution not complete.
[c]Values at TSGC-RNA/H = 30, evolution not complete.
[d]Values at TS1-RNA/HT = 21, evolution not complete.

The emission enhancement rates, i.e. the increase in the emission band areas with increasing nucleic acid (NA)/HT ratios, were larger for the three RNA-HT complexes than for the GC-DNA-HT complex, and all of them were much lower than that for the AT-DNA-HT minor groove complex (see the $A^f_{HT/NA}/A^f_{HT}$ ratios in Table 1). In addition, the area plots in the insets (Figure 5A; Supplementary Figures S8 and S9) showed some downward curvatures for the three RNAs, but not for GC-DNA (Supplementary Figure S7) at similar NA/HT ratios. This indicates slightly higher stabilities of the fluorescent complexes obtained with the RNAs than with GC-DNA.

The most striking resemblance between the properties of the complexes with GC-DNA and the three RNAs concerns the fluorescence lifetimes, all between 4.1 and 4.3 ns (Table 1). These relatively long lifetimes indicate a loss of torsional freedom of HT in the complexes,

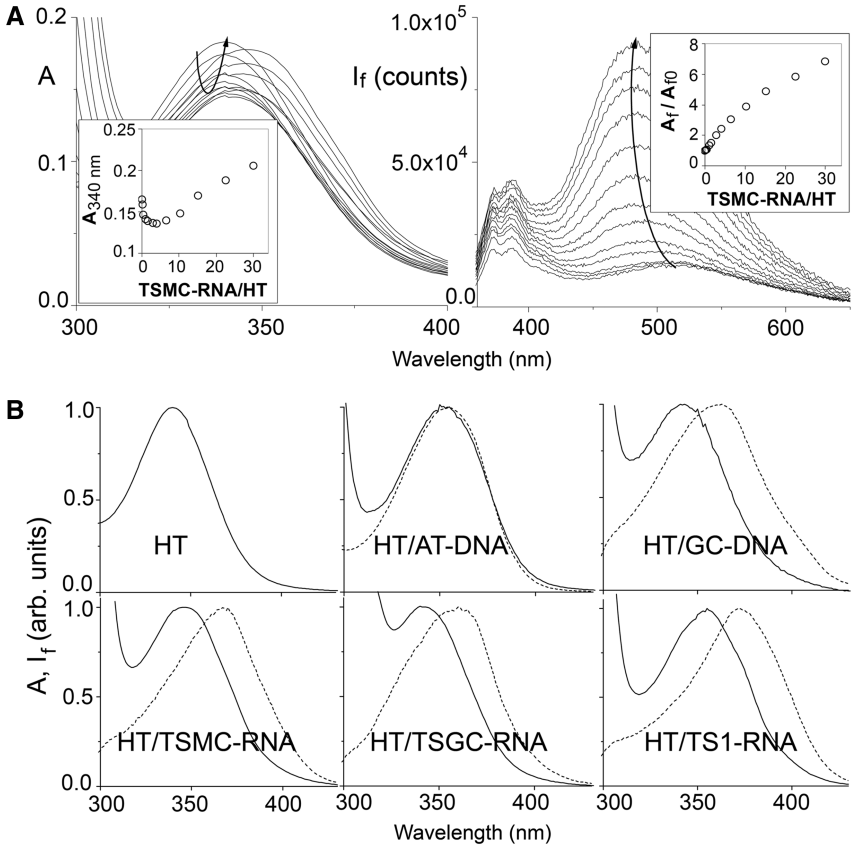

Figure 5. (A) Absorption (left) and fluorescence emission (right) evolutions of HT titrated with TSMC-RNA. Insets: absorbance at 340 nm (left) and relative emission band (right) areas (both corrected for dilution) as functions of the TSMC-RNA/HT mole ratio. Excitation wavelength: 330 nm (see Supplementary data for details). **(B)** Absorption (solid lines) and fluorescence excitation (dashed lines) spectra of HT alone and titrated with AT-DNA, GC-DNA, TSMC-RNA, TSGC-RNA and TS1-RNA at the largest NA/HT mole ratios attained (see text and Table 1). Emission wavelengths are 490 nm for HT alone, 450 nm for HT/AT-DNA and 480 nm for the other complexes.

consistent, as for GC-DNA, with an intercalative binding. On the other hand, the fluorescence excitation and, to a lesser extent, the absorption and emission spectra revealed some differences between the emitting complexes obtained with the three RNAs. Both the absorption and the excitation band maxima exhibited a progressive blue shift on moving from TS1 (355 and 372 nm) to TSMC (346 and 367 nm) to TSGC (342 and 360 nm). The emission maxima exhibited a similar, though less pronounced blue shift: 485, 483 and 480 nm. Since absorption band shifts and intensity changes are connected with the nature and geometries of the possibly many (28), aggregated forms that prevail at low NA/H ratios, and with the details of the exciton interactions between the chromophores in these aggregates, an interpretation of this property seems impossible, and of limited interest, at this stage. On the other hand, the positions of the excitation spectra are specific features of the single emitting complex which prevails at high RNA/HT ratios. Different shifts in these spectra can be interpreted both in terms of differences in absorption solvatochromism and of different degrees of coplanarity of the two benzimidazole subunits of HT in the intercalation complexes. Under the assumption of a reduced accessibility of water to the complexed dye as compared with free HT, negative solvatochromism of HT has often been invoked, to account for the absorption red shift (+12 nm; Table 1) of minor-groove complexes of HT with AT-DNAs. However, intercalation might also induce a distortion of HT with a change in geometry, particularly concerning the intramolecular torsional coordinate, thereby affecting the absorption and emission spectra. In this respect, the observed blue shifts in the excitation spectra would indicate increasing exposure to water and/or increasing distortion of intercalated HT in the TS1-TSMC-TSGC RNA series.

A possible mechanism for HT-TSMC intercalation

From UV-Vis and fluorescence spectroscopy, it is clear that HT binds the RNAs studied in more than one way, but it is also clear that there is a preference for intercalation of HT at low HT/RNA ratios. In HT, the chromophoric bis-benzimidazole fragment (Figure 1C, rings R2 and R3) is flanked by rings R1 and R4 on either side, making it nearly impossible for the chromophoric fragment to intercalate without piercing through the RNA helix. Since there are no available experimentally determined structures showing such a binding mode, we performed molecular docking and MDs simulations to investigate the mechanism by which HT might intercalate. Docking of HT to the CC mismatch region of TSMC was

performed as described in the 'Methods' section. Two poses, A and B (Supplementary Figure S1), were generated by docking in which HT lay in the major groove in opposite directions (related by 180° rotation). In the A pose, ring R4 was pointed toward C16 of TSMC, and R1 was oriented toward C5. In the B pose, ring R1 was oriented toward C16, while R4 was toward C5. These two docking poses were used as starting structures for independent MDs simulations.

During the first step of the two step simulation protocol employed, the RNA was restrained while HT was free to move (see 'Methods' section for details). In the simulation starting with pose A, HT remained in the major groove in contact with the RNA throughout the simulation and the interactions between TSMC and HT were optimized. In the simulation starting with HT docked in pose B, HT was released into solvent during the first nanosecond of the simulation (see Supplementary Data Discussion). Therefore, pose B was discarded, and the final structure from the simulation with pose A, A1, was used as the starting structure in simulation A2, in which the CC mismatch, one flanking base pair on either side of the mismatch and HT were free while the rest of the RNA was restrained (see 'Methods' section for details). To our surprise, during simulation A2, HT indeed penetrated through the helix, thus adopting an intercalative binding mode. An interesting chain of events (Figure 6) led to this induced fit intercalative binding mode (Figure 2B). HT slid over the furrow in the surface formed by the CC mismatch such that HT-H6 of the ring R1 could make a H-bond with the backbone C5-O2P. While the ring R1 was so anchored, a rotation, driven by the possibility of H-bonding between HT-H3 and TSMC-G17-O6, occurred at the γ bond (Figure 1B and C) between 7 and 9 ns. This was followed by the formation of a H-bond between HT-H1 and the backbone TSMC-G17-O2P at 9.2 ns. Simultaneously, the TSMC-C16 base began to flip out to stack against the ring R2 of HT. Stacking against C16 and H-bonding between HT-N3 and TSMC-G17-N7 were the key interactions that permitted HT to reorient and penetrate through the helix, ring R1 first, at 11.2 ns.

It is imperative to mention that the simulation A2 was run for only 24.6 ns, implying insufficient sampling to establish the binding mode definitively. At the same time, it is difficult to sample completely enough to establish the binding mode. Therefore, the induced-fit mechanism of intercalation discussed here may not be the main method of interaction, rather, it represents one possible interaction mode.

Validation of the intercalation binding model

Structural stability induced upon intercalation

HT began intercalating into the CC mismatch only after ~9 ns of the A2 simulation. In the preceding period, the interactions of HT in the major groove and its alignment with the mismatch were adjusted to allow for the

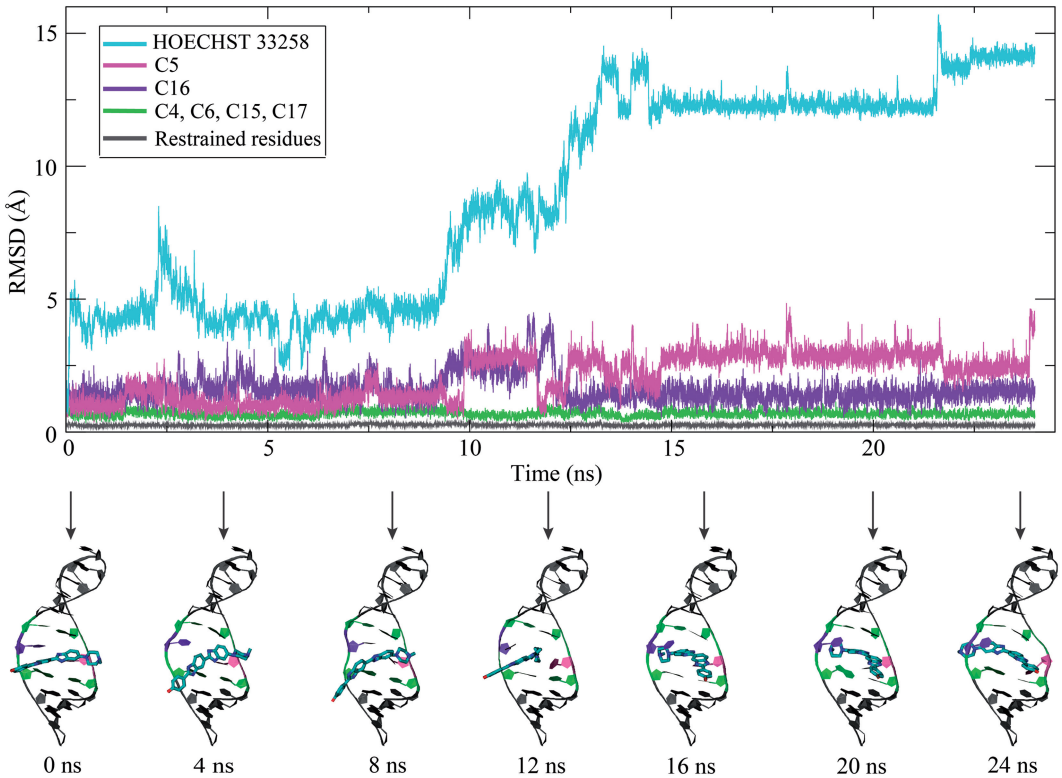

Figure 6. Top: RMSD versus time plot for TSMC residues and HT during simulation A2. C5 and C16 are the residues in the mismatch, C4, G6, C15 and G17 are the residues flanking the mismatch in the stem; all these were unrestrained during the simulation. Restrained residues refer to the remaining residues of TSMC. Bottom: Snapshots of the HT-TSMC complex at various timepoints during the simulation. TSMC is shown in cartoon, whereas HT is shown in stick representation. The residues are colored by same scheme as in the RMSD plot.

subsequent intercalation. It can be considered that the period up to ~9 ns represents the interactions of HT with the major groove, without any intercalative component. Fluctuating root mean square deviation (RMSD) values for HT (Figure 6) during this time suggest that binding in the major groove did not lead to a very stable complex. High fluctuations in the RMSD of C5, C16 and HT during the 9–15 ns period represent the intercalating event. Thereafter, the RMSD values stabilize indicating formation of a structurally stable intercalated complex. At ~21.5 ns, the intercalated HT slid further into the binding pocket formed to optimize the stacking against bases C4, C5, G6, C16 and G17. The phenolic hydroxyl group on HT shifted from H-bonding to C3-O2P to C4-O2P. C5 also slightly readjusted for better stacking.

The reduced mobility of HT upon intercalation as compared with groove binding was also evident from the change in atomic RMS fluctuations (RMSF) for HT, which reduced from 163 Å during the first 9 ns of the simulation to 16 Å toward the end and after discounting the sliding event at 21.5 ns. Similarly to HT, the CC mismatch of the RNA also experienced improved structural stability upon intercalation (Supplementary Figure S10). In free (unliganded) TSMC, the mismatch residues C5 and C16 had high RMSF of 42 and 38 Å, respectively. During the first 9 ns of simulation A2, i.e. before initiation of HT intercalation, the RMSF of C5 had decreased to 22 Å, whereas C16 was almost unaltered at 41 Å. After intercalation, i.e. 15–24.6 ns, the RMSF of C5 increased slightly to 26 Å; however, RMSF of C16 reduced significantly to 19 Å, implying that C16 was additionally stabilized by intercalation of HT as compared with earlier when HT was interacting with the major groove. Irrespective of the presence or the binding mode of HT, the flanking base pairs above and below the CC mismatch i.e. C4, G6, C15 and G17, which were also allowed unrestrained movement in the A2 simulation, continued fluctuating to a similar extent as in the free TSMC.

Intercalation is the energetically favorable binding mode

Since it was of interest to deduce the effect of intercalation on the binding free energy of the complex, the trajectory A2 was split into segments of 5 ns each; the first two segments representing the major groove binding mode, the last two segments representing intercalation. When the HT interactions were limited to the major groove, e.g. during the first 5 ns, the computed binding free energy was only −13.7 kcal/mol, whereas upon intercalation i.e. during the last two segments at 15–20 ns and 20–24.6 ns, it improved significantly to ~−30 kcal/mol (Table 2). Therefore, compared with binding in the major groove, the intercalative mode is energetically more favorable.

Solvent exposure and structural rigidity of HT bis-benzimidazole subunit

The solvent exposed surface area (SASA) and torsional rigidity of the HT bis-benzimidazole fragment, i.e. rings R2 and R3 (Figure 1C), are responsible for the measured absorption and fluorescence properties of HT. An analysis of these structural properties was performed to examine the consistency of the simulated model with the experimental data. In free HT, the average computed SASA of the chromophoric fragment was 280 Å^2, while a reduction in SASA was observed upon binding TSMC (Supplementary Figure S11). For the first 11 ns of simulation A2, i.e. during binding in the major groove and a part of the transition toward intercalation, the SASA of the bis-benzimidazole fragment could be broadly divided into two clusters, at 160 and 260 Å^2; but by the time of stabilization of intercalation at 15 ns, the SASA had decreased significantly to 65 Å^2.

Table 2. Computed binding free energy of the HT-TSMC complex, calculated with a continuum solvent model (PBSA) for consecutive segments of the simulated trajectory

Time frame (ns)	ΔE_{vdw} (kcal/mol)	$\Delta E_{Electrostatic}$ (kcal/mol)	ΔG_{PB} (kcal/mol)	ΔG_{SA} (kcal/mol)	Binding free energy (kcal/mol)
0–5	−21.3 ± 4.6	−530.0 ± 10.4	539.5 ± 11.3	−2.0 ± 0.5	−13.7 ± 3.2
5–10	−25.1 ± 3.2	−545.1 ± 14.6	552.4 ± 13.5	−2.1 ± 0.2	−19.9 ± 5.2
10–15	−33.6 ± 9.7	−467.5 ± 63.1	480.7 ± 56.0	−2.2 ± 0.6	−22.6 ± 3.8
15–20	−45.4 ± 2.6	−446.6 ± 8.1	465.3 ± 7.4	−3.3 ± 0.1	−30.0 ± 2.9
20–24.6	−44.9 ± 2.7	−425.1 ± 19.3	442.2 ± 19.2	−3.1 ± 0.2	−30.9 ± 2.9

During the simulation of free HT, the torsion angle β between the rings R2 and R3 fluctuates around two values: 1° ± 19° and 181° ± 17° (Supplementary Figure S12), indicating free rotation around the bond between the two favored planar geometries. However, after binding the RNA, such rotation was inhibited and the torsion angle β fluctuated at −5° ± 17° for the complete run. Moreover, the magnitude of the fluctuation of the β torsion angle was slightly reduced upon intercalation, −7° ± 13° during 15–24.6 ns, compared with groove binding, −4° ± 19° during 0–9 ns, although the effect was not as prominent as for the SASA. These data, especially for the intercalation binding mode, are consistent with the reduced solvent exposure and increased rigidity of HT observed in UV-visible and fluorescence experiments.

Based on the analysis of the MD data, the decreasing magnitude of changes in the fluorescence properties of HT when bound to TS1 > TSMC > TSGC can also be rationalized. Each helical turn of an A-form RNA helix consists of 10–11 base pairs. Therefore, the TS1 stem, which consists of 12 base pairs, incorporates a complete turn, whereas TSMC, with a stem of 8 base pairs, does not. This implies a deeper major groove for TS1, capable of shielding HT from solvent better than TSMC, in both groove and intercalative binding modes. Due to the absence of the CC mismatch, intercalation would be less feasible in TSGC and groove binding would be expected to predominate. Therefore, the SASA of the HT choromophore, though less than in free HT, would not reduce as much as in TS1 or TSMC where intercalation is more feasible.

In the structural model presented here (Figure 2B), the methylpiperazine moiety (ring R1) of HT protrudes into the minor groove, whereas the phenolic moiety (ring R4) points toward the major groove of the RNA. It would be

logical to expect that a model with the reverse orientation, i.e. ring R4 protruding into the minor groove while the ring R1 extended toward the major groove would be an equally feasible option. In such a structure, HT-H6 could form a hydrogen bond with the backbone phosphate groups of C3 or C4 and ring R4 could shield the C4 of TSMC from solvent. Although such a model could be energetically favorable, our NMR data argue against this mode of binding. Depending on the rate of exchange between the free and bound forms, the ^{1}H NMR signals of HT would shift or broaden out. This effect would be more pronounced for the protons making direct contacts with the RNA. In the NMR spectrum, the protons from aromatic rings R2, R3 and R4 of HT resonate between 6.5 and 7.5 ppm, whereas the aliphatic protons for the methyl group attached to R1 appear at 2.8 ppm. During titrations of HT into RNA, the signals for the methyl protons in R1 built up with increasing concentrations of HT whereas the signals of the aromatic protons remain broadened beyond detection (Supplementary Figure S13A). Similarly, in the TOCSY spectra recorded for free HT in $^{2}H_2O$ and subsequent titrations of TSMC into HT, the signals for the aromatic rings of HT were bleached upon the first instance of RNA addition, with an HT:RNA ratio of 1:0.25, whereas the signals from R1 were neither shifted nor significantly broadened (Supplementary Figure S13B). These observations suggest that ring R1 of HT is relatively free and not involved in interactions with TSMC. Therefore, the orientation of the intercalated HT should be as proposed by our model and not the one flipped by 180°.

Summary and conclusions

Development of resistance due to overexpression of TS protein is a problem associated with most of the drugs inhibiting the TS protein. Targeting the TS mRNA could provide a means to tackle this problem. The biological assays characterizing TS protein and TS mRNA levels in cells treated by HT showed that HT treatment resulted in a reduction in TS protein levels without altering the TS mRNA levels, indicating that HT modulates TS expression by interfering with TS translation. Therefore, although HT itself is not a good drug candidate, its biological activity suggests that it could be used as a lead molecule to design drugs targeting the TS mRNA. Since structural information on the TS mRNA-HT complex could tremendously aid these drug design efforts, we obtained insights into the complex formation using the TSMC RNA construct as a model for the Site I of TS mRNA. Although the existence of more than one binding mode was observed for the TSMC-HT complex, NMR, UV-Vis and fluorescence spectroscopy based evidence support intercalation as the dominant binding mode at low TSMC/HT ratios. The structural model developed using docking and MDs simulations confirmed that intercalation at the CC mismatch in the RNA is sterically feasible and energetically favorable compared with the alternative possibility of groove binding.

SUPPLEMENTARY DATA

Supplementary Data are available at NAR Online: Supplementary Figures 1–13, Supplementary Discussion and Supplementary References [29–31].

ACKNOWLEDGEMENTS

We thank Prof. S.A. Corcelli for providing the parameters for HT for the molecular simulations. We acknowledge the support of Leibniz Supercomputing Centre (LRZ). We also thank Christina Siedler for help with transferring the published assignments to our spectra. M.P.C. acknowledges the support of the Italian Association for cancer research (AIRC)-DROC IG 10474.

FUNDING

The European Union [FP6 STREP project LIGHTS LSH-2005-2.2.0-8]; Klaus Tschira Foundation; Graduiertenkolleg 'Integrated Analysis of Macromolecular Complexes and Hybrid Methods in Genome Biology' [GRK1721]; Sonderforschungsbereich 1035 'Control of protein function by conformational switching' [SFB1035]. Funding for open access charge: HITS/Klaus Tschira Foundation.

Conflict of interest statement. None declared.

REFERENCES

1. Garg,D., Henrich,S., Salo-Ahen,O.M., Myllykallio,H., Costi,M.P. and Wade,R.C. (2010) Novel approaches for targeting thymidylate synthase to overcome the resistance and toxicity of anticancer drugs. *J. Med.Chem.*, **53**, 6539–6549.
2. Chu,E., Koeller,D.M., Casey,J.L., Drake,J.C., Chabner,B.A., Elwood,P.C., Zinn,S. and Allegra,C.J. (1991) Autoregulation of human thymidylate synthase messenger RNA translation by thymidylate synthase. *Proc. Natl Acad. Sci. USA*, **88**, 8977–8981.
3. Chu,E., Voeller,D., Koeller,D.M., Drake,J.C., Takimoto,C.H., Maley,G.F., Maley,F. and Allegra,C.J. (1993) Identification of an RNA binding site for human thymidylate synthase. *Proc. Natl Acad. Sci. USA*, **90**, 517–521.
4. Cho,J. and Rando,R.R. (2000) Specific binding of Hoechst 33258 to site 1 thymidylate synthase mRNA. *Nucleic Acids Res.*, **28**, 2158–2163.
5. Tok,J.B., Cho,J. and Rando,R.R. (1999) Aminoglycoside antibiotics are able to specifically bind the 5'-untranslated region of thymidylate synthase messenger RNA. *Biochemistry*, **38**, 199–206.
6. Tavares,T.J., Beribisky,A.V. and Johnson,P.E. (2009) Structure of the cytosine-cytosine mismatch in the thymidylate synthase mRNA binding site and analysis of its interaction with the aminoglycoside paromomycin. *RNA*, **15**, 911–922.
7. Vega,M.C., Garcia Saez,I., Aymami,J., Eritja,R., Van der Marel,G.A., Van Boom,J.H., Rich,A. and Coll,M. (1994) Three-dimensional crystal structure of the A-tract DNA dodecamer d(CGCAAATTTGCG) complexed with the minor-groove-binding drug Hoechst 33258. *Eur. J. Biochem.*, **222**, 721–726.
8. Adhikary,A., Buschmann,V., Muller,C. and Sauer,M. (2003) Ensemble and single-molecule fluorescence spectroscopic study of the binding modes of the bis-benzimidazole derivative Hoechst 33258 with DNA. *Nucleic Acids Res.*, **31**, 2178–2186.
9. Bailly,C., Colson,P., Henichart,J.P. and Houssier,C. (1993) The different binding modes of Hoechst 33258 to DNA studied by electric linear dichroism. *Nucleic Acids Res.*, **21**, 3705–3709.

10. Colson,P., Houssier,C. and Bailly,C. (1995) Use of electric linear dichroism and competition experiments with intercalating drugs to investigate the mode of binding of Hoechst 33258, berenil and DAPI to GC sequences. *J. Biomol. Struct. Dyn.*, **13**, 351–366.
11. Bailly,C., Colson,P., Houssier,C. and Hamy,F. (1996) The binding mode of drugs to the TAR RNA of HIV-1 studied by electric linear dichroism. *Nucleic Acids Res.*, **24**, 1460–1464.
12. Baraldi,P.G., Bovero,A., Fruttarolo,F., Preti,D., Tabrizi,M.A., Pavani,M.G. and Romagnoli,R. (2004) DNA minor groove binders as potential antitumor and antimicrobial agents. *Med. Res. Rev.*, **24**, 475–528.
13. Persson,L. and Pegg,A.E. (1984) Studies of the induction of spermidine/spermine N^1-acetyltransferase using a specific antiserum. *J. Biol. Chem.*, **259**, 12364–12367.
14. Lowry,O.H., Rosebrough,N.J., Farr,A.L. and Randall,R.J. (1951) Protein measurement with the Folin phenol reagent. *J. Biol. Chem.*, **193**, 265–275.
15. Arocho,A., Chen,B., Ladanyi,M. and Pan,Q. (2006) Validation of the 2-DeltaDeltaCt calculation as an alternate method of data analysis for quantitative PCR of BCR-ABL P210 transcripts. *Diagn. Mol. Pathol.*, **15**, 56–61.
16. Piotto,M., Saudek,V. and Sklenar,V. (1992) Gradient-tailored excitation for single-quantum NMR spectroscopy of aqueous solutions. *J. Biomol. NMR*, **2**, 661–665.
17. Sklenar,V., Piotto,M., Leppik,R. and Saudek,V. (1993) Gradient-tailored water suppression for 1H-15N HSQC experiments optimized to retain full sensitivity. *J. Magn. Reson. Ser. A*, **102**, 241–245.
18. Liu,M., Mao,X.-A., Ye,C., Huang,H., Nicholson,J.K. and Lindon,J.C. (1998) Improved WATERGATE Pulse Sequences for Solvent Suppression in NMR Spectroscopy. *J. Magn. Reson.*, **132**, 125–129.
19. Furse,K.E., Lindquist,B.A. and Corcelli,S.A. (2008) Solvation dynamics of Hoechst 33258 in water: an equilibrium and nonequilibrium molecular dynamics study. *J. Phys. Chem. B*, **112**, 3231–3239.
20. Perez,A., Marchan,I., Svozil,D., Sponer,J., Cheatham,T.E. 3rd, Laughton,C.A. and Orozco,M. (2007) Refinement of the AMBER force field for nucleic acids: improving the description of alpha/gamma conformers. *Biophys. J.*, **92**, 3817–3829.
21. Case,D.A., Cheatham,T.E. 3rd, Darden,T., Gohlke,H., Luo,R., Merz,K.M. Jr, Onufriev,A., Simmerling,C., Wang,B. and Woods,R.J. (2005) The Amber biomolecular simulation programs. *J. Comput. Chem.*, **26**, 1668–1688.
22. Jorgensen,W.L. (1982) Revised TIPS for simulations of liquid water and aqueous solutions. *J. Chem. Phys.*, **77**, 4156–4163.
23. Ryckaert,J.-P., Ciccotti,G. and Berendsen,H.J.C. (1977) Numerical intergration of the cartesian equations of motion of a system with constraints: molecular dynamics of n-alkanes. *J. Comp. Phys.*, **23**, 327–341.
24. Shields,G.C., Laughton,C.A. and Orozco,M. (1997) Molecular dynamics simulations of the d(T•A•T) triple helix. *J. Am. Chem. Soc.*, **119**, 7463–7469.
25. Berendsen,H.J.C., Postma,J.P.M., van Gunsteren,W.F., DiNola,A. and Haak,J.R. (1984) Molecular dynamics with coupling to an external bath. *J. Chem. Phys.*, **81**, 3684–3690.
26. Hasnat,A., Bichenkova,E., Yu,X., Arnold,J.R., Fisher,J., Fedorova,O. and Andrews,J. (2007) Fluorescence spectroscopic and (19)f NMR studies of human thymidylate synthase with its cognate RNA. *J. Biomol. Struct. Dyn.*, **25**, 253–270.
27. Dibrov,S., McLean,J. and Hermann,T. (2011) Structure of an RNA dimer of a regulatory element from human thymidylate synthase mRNA. *Acta Crystallogr. D Biol. Crystallogr.*, **67**, 97–104.
28. Loontiens,F.G., Regenfuss,P., Zechel,A., Dumortier,L. and Clegg,R.M. (1990) Binding characteristics of Hoechst 33258 with calf thymus DNA, poly[d(A-T)], and d(CCGGAATTCCGG): multiple stoichiometries and determination of tight binding with a wide spectrum of site affinities. *Biochemistry*, **29**, 9029–9039.
29. Cosa,G., Focsaneanu,K.S., McLean,J.R., McNamee,J.P. and Scaiano,J.C. (2001) Photophysical properties of fluorescent DNA-dyes bound to single- and double-stranded DNA in aqueous buffered solution. *Photochem. Photobiol.*, **73**, 585–599.
30. Utsuno,K., Maeda,Y. and Tsuboi,M. (1999) How and how much can Hoechst 33258 cause unwinding in a DNA duplex? *Chem. Pharm. Bull. (Tokyo)*, **47**, 1363–1368.
31. Caselli,M., Latterini,L. and Ponterini,G. (2004) Consequences of H-dimerization on the photophysics and photochemistry of oxacarbocyanines. *Phys. Chem. Chem. Phys.*, **6**, 3857–3863.